

Adaptive Near-Optimal Compensation in Lossy Polyphase Power Systems

Hanoch Lev-Ari, *Fellow, IEEE*, Ronald D. Hernández, *Graduate Student Member, IEEE*, Aleksandar M. Stanković, *Fellow, IEEE*, and Edwin A. Marengo, *Senior Member, IEEE*

Abstract—The paper provides a formulation and solution for the problem of optimizing power flows in polyphase power systems with significant source (line) impedance. An optimal solution considering significant line impedance has been already obtained in recent works. Unfortunately, it relies on network and load parameters that are not easy to determine during operation. This motivates our approach in searching for a sub-optimal easy-to-implement solution that relies only on measurements of the load voltage and current so as to allow precise control of the compensated load as well as the real power flowing out of the compensator, while reducing line losses to within a few percent of its theoretical minimum. Properties of the solution are illustrated for an asymmetrical three phase induction motor supplied with unbalanced non-sinusoidal voltages.

Index Terms—Compensation, Hilbert spaces, optimization methods.

I. INTRODUCTION

IN this paper we develop an adaptive procedure for power compensation in systems with significant equivalent source impedance. We consider a realistic scenario involving general polyphase systems with harmonics, and our near-optimal procedure does not require extensive knowledge of system parameters.

Significant source impedance is common in spatially extended networks such as those in rural and suburban areas. It is also present in the emerging class of micro-grids that combine distributed sources and loads. Variations in the equivalent source impedance are also increasingly common due to more frequent switching of components in transmission and distribution systems that include distributed energy resources.

The effects of source impedance on power transfer are twofold: it reduces the efficiency of the energy transfer and it may lead to instabilities due to resonances and other unexpected interactions between the impedance and the system components [1]. Additionally, large source impedance and unbalance may complicate local control of power electronic converters [2].

The role of compensation in power system efficiency optimization is to reduce the power consumption of the Thevenin equivalent source (or “line”) impedance, so that most of the source power is delivered to the load (Fig. 1). A classical result by Fryze [3] states that when the voltage drop across the line

impedance is negligible in comparison with the load voltage, i.e., when $\|v_s(t) - v(t)\| \ll \|v(t)\|$ then the smallest possible source current $i_s(t)$ (in rms) is

$$i_F(t) = \frac{P_{load}^{(u)}}{\|v\|^2} v(t)$$

where $P_{load}^{(u)}$ is the original real (average) power delivered to the load without compensation (uncompensated load), and $\|v\|$ denotes the rms value of a waveform $v(t)$. Recently we have put compensation (with negligible voltage drop) in a convenient geometric (Hilbert space) setting, and determined optimal solutions under unequal line resistances and bandwidth limitation on the compensator current [4–6].

However, when the source impedance becomes significant (namely, a few percent of the load impedance, or higher) the traditional Fryze current is no longer the smallest (by rms) line current that supplies the same real power to the load as the original load current. In that case, every adjustment in the compensator current results in a change of voltage load, which in turn, requires further adjustments in compensator current. Furthermore, the theoretically-optimal compensator, as derived in [7], [8], depends on both the equivalent source impedance and the current-voltage characteristic of the load. Such information is usually difficult to obtain, especially in view of the time-varying nature of network parameters. The knowledge of the achievable (optimal) system compensation is important in all electric energy systems, as it establishes limits of technical performance that can be used as a yardstick for ranking different compensation methods. A summary of relevant concepts and results from [7], [8] is provided in Sec. III.

The compensation setup that we consider is similar to the one addressed in [9]. However, our solution does not require knowledge of all network parameters, as we achieve robustness through adaptation. This may prove advantageous in applications, as the behavior of actual systems often includes significant parameter variations at different frequencies and at different operating conditions [10]. Our solution points out to need for real-time collaboration and coordination between the electric energy supplier (e.g., a utility) and loads in the sense that optimal compensation requires adjustments of both load current (commonly considered the purview of the customer [11] and of the source voltage (typically the domain of the supplier). Our findings are consistent with results reported in [12], [13] that stress the need for collaborative control in efficiency-optimized energy networks.

This work was supported in part by the National Science Foundation under Grants ECS-0601256 and ECS-0746310.

The authors are with the Department of Electrical and Computer Engineering, Northeastern University, Boston, MA, 02115 USA (e-mail: levvari@ece.neu.edu; rhermand@ece.neu.edu; astankov@ece.neu.edu; emarengo@ece.neu.edu).

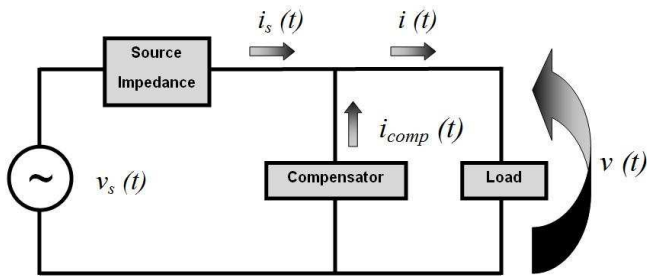


Fig. 1. Load compensation in a power delivery system.

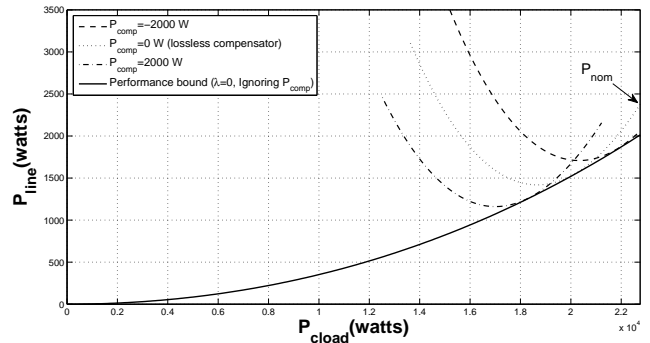
In this paper we introduce an adaptive near-optimal compensation scheme that relies only on measurements of the load voltage and current or, equivalently, on the phasor description of these waveforms. Our compensator tracks variations in both network and load conditions, continuously adjusting the polyphase waveform $i_{comp}(t)$ so as to reduce the power dissipated in the source impedance, for both linear and nonlinear loads. To be specific, this compensation algorithm allows precise control of P_{comp} , the real power flowing out of the compensator, as well as P_{load} , the real power delivered to the compensated load (i.e., $P_{load} = P_{load} - P_{comp}$), while reducing P_{line} , the power dissipated in the source impedance, to within a few percent of its theoretical minimum. Normally we set $P_{comp} = 0$, but other “target” values are possible.

The heart of our adaptive compensation scheme is the concept of *quadrature Fryze* compensation (*quad-Fryze* for short), which was introduced in [7]. The objective of a quad-Fryze compensator is to adjust $i_{comp}(t)$ so that the compensated load is linear and time-invariant with a current-voltage characteristic given by

$$i_s(t) = \alpha v(t) - \beta \mathcal{H}\{v(t)\}. \quad (1)$$

Here α, β are real-valued coefficients and $\mathcal{H}\{\cdot\}$ represents the Hilbert transform of a signal. In other words, the compensated line current is a linear combination of the load voltage $v(t)$ and its Hilbert transform $\mathcal{H}\{v(t)\}$. We call this compensation method “quadrature Fryze” because the Hilbert transform imparts a 90° phase delay to $v(t)$. It was demonstrated in [7] that the performance of this (implicit) compensation scheme is often very close to the theoretical optimum even in the presence of significant source impedance. A detailed discussion of the quad-Fryze compensation method is provided in Sec. IV.

We evaluate the performance of our adaptive compensation scheme by comparing it with the theoretical optimum, using results from [8]. In particular, we use the *universal performance bound*, as well as several *cross-section* curves (Fig. 2) obtained by imposing a constraint on the value of P_{comp} . The construction of such optimal performance curves requires explicit knowledge of network and load parameters (see details in Sec. III). Each cross-section curve describes the theoretical minimum for P_{line} as a function of P_{load} for a prescribed level of P_{comp} . Naturally, our primary interest in steady-state is the cross-section curve for $P_{comp} = 0$ (the

Fig. 2. Optimal performance benchmarks ($P_{nom} = 22,750W$).

dotted line in Fig. 2). The universal performance bound (solid line in Fig. 2) describes the theoretical minimum for P_{line} as a function of P_{load} , with no constraints on P_{comp} . Thus this bound is the lower boundary for all cross-section curves: points below this boundary are not feasible for the given (polyphase) source voltage and impedance.

The two parameters α and β in (1) can be used to control the values of P_{comp} and P_{load} . Our adaptive compensation algorithm adjusts these two control parameters to achieve the prescribed P_{comp}, P_{load} values, relying in the process only on dynamic phasor information about the load current and voltage (see Sec. V for details).

Our adaptive compensation scheme maintains $P_{comp} \approx 0$ at all times, and converges, under steady-state network and load conditions to $P_{comp} = 0$,¹ while reducing the energy loss in the line very nearly to its theoretical minimum. In addition, the algorithm can be adaptively steered to adjust P_{load} to any desired value up to P_{nom} , the nominal power that would be delivered to the load in the absence of any line/source impedance. Notice that prescribing a P_{load} value near P_{nom} must come at the cost of increased P_{line} , as is evident from the cross-section curves in Fig. 2.

The remainder of the paper is organized as follows. In Sec. II we formulate the adaptive compensation problem using concepts and results from [4–7]. The most important of these concepts are the quad-Fryze compensator, which we describe in detail in Sec. IV, and optimal performance curves, which are introduced in Sec. III. We demonstrate in Sec. V that the performance of our adaptive compensation algorithm remains close to optimum both during the convergence stage and in steady-state. Finally, we provide concluding remarks in Sec. VI.

II. PROBLEM FORMULATION

The Hilbert space terminology of [4] is used here to formulate our objectives and derive our results. Thus $v(t)$ and $i(t)$ are row vectors representing polyphase load voltage and current, respectively, which we view as elements in a Hilbert space of n -phase, T -periodic, square-integrable waveforms,

¹Alternatively, one can prescribe any desired (non-zero) value for P_{comp} .

with the inner product represented by

$$\langle x, y \rangle \stackrel{\text{def}}{=} \frac{1}{T} \int_T x(t)y(t)^\top dt \quad (2)$$

where the superscript \top denotes transposition.

This inner product can also be evaluated in terms of the Fourier coefficients X_l , Y_l of the polyphase waveforms $x(t)$, $y(t)$, namely

$$\langle x, y \rangle = \Re\{\mathcal{X}\mathcal{Y}^H\} \quad (3a)$$

where the subscript H indicates conjugate transpose, and \mathcal{X} is a one-sided phasor array, viz.,

$$\mathcal{X} \stackrel{\text{def}}{=} [X_0 \quad \sqrt{2}X_1 \quad \sqrt{2}X_2 \quad \dots] \quad (3b)$$

consisting of the row-vector Fourier coefficients

$$X_l = \frac{1}{T} \int_T x(t)e^{-j\omega_l t} dt \quad (3c)$$

and similarly for the phasor array \mathcal{Y} , which represents the waveform $y(t)$.

The behavior of the power delivery system of Fig. 1 is determined by the current-voltage characteristic of the load and the (frequency-domain) circuit equations

$$\mathcal{I} = \mathcal{I}_s + \mathcal{I}_{comp} \quad (4a)$$

$$\mathcal{V} = \mathcal{V}_s - \mathcal{I}_s \mathcal{Z}_s \quad (4b)$$

where \mathcal{Z}_s is a complex-valued matrix representing the linear time-invariant source impedance, and \mathcal{I} , \mathcal{I}_s , \mathcal{I}_{comp} , \mathcal{V} , \mathcal{V}_s are the phasor arrays associated with the polyphase waveforms $i(t)$, $i_s(t)$, $i_{comp}(t)$, $v(t)$, $v_s(t)$, respectively.

These circuit equations establish a one-to-one correspondence between the source current \mathcal{I}_s and the compensator current \mathcal{I}_{comp} (when we consider a fixed \mathcal{V}_s , \mathcal{Z}_s and \mathcal{Y}). This is straightforward to establish for a linear load, where $\mathcal{I} = \mathcal{V}\mathcal{Y}$ with the matrix \mathcal{Y} representing the load admittance. Indeed, from (4) we can get

$$\mathcal{I}_s = (\mathcal{V}_s - \mathcal{I}_s \mathcal{Z}_s)\mathcal{Y} - \mathcal{I}_{comp}$$

so that

$$\mathcal{I}_s = (\mathcal{V}_s \mathcal{Y} - \mathcal{I}_{comp})(I + \mathcal{Z}_s \mathcal{Y})^{-1} \quad (5a)$$

and

$$\begin{aligned} \mathcal{V} &= \mathcal{V}_s - \mathcal{I}_s \mathcal{Z}_s \\ &= (\mathcal{V}_s + \mathcal{I}_{comp} \mathcal{Z}_s)(I + \mathcal{Y} \mathcal{Z}_s)^{-1}. \end{aligned} \quad (5b)$$

In the linear case, nonsingularity of the matrix $(I + \mathcal{Z}_s \mathcal{Y})$ is the only condition needed to ensure one-to-one correspondence between \mathcal{I}_s and \mathcal{I}_{comp} . This condition is almost always met, either because $\|\mathcal{Z}_s \mathcal{Y}\|$ is small, or because the eigenvalues of $\mathcal{Z}_s \mathcal{Y}$ have a positive real part (see Appendix A for further details).

The performance of any compensator, including the one we introduce in this paper, can be evaluated in terms of three real (average) power quantities:

- The power P_{line} dissipated in the equivalent source impedance, viz.,

$$P_{line} \stackrel{\text{def}}{=} \mathcal{I}_s \mathcal{R}_s \mathcal{I}_s^H \quad (6a)$$

where

$$\mathcal{R}_s \stackrel{\text{def}}{=} \frac{1}{2} \{\mathcal{Z}_s + \mathcal{Z}_s^H\}. \quad (6b)$$

- The power P_{load} delivered to the compensated load, viz.,

$$P_{load} \stackrel{\text{def}}{=} \Re\{\mathcal{I}_s \mathcal{V}^H\} = \Re\{\mathcal{I}_s \mathcal{V}_s^H\} - P_{line}. \quad (7)$$

- The power P_{comp} flowing out of the compensator, viz.,

$$\begin{aligned} P_{comp} &\stackrel{\text{def}}{=} \Re\{\mathcal{I}_{comp} \mathcal{V}^H\} \\ &= \Re\{\mathcal{I} \mathcal{V}^H\} - P_{load}. \end{aligned} \quad (8)$$

Notice that our expressions use \mathcal{I}_s , rather than \mathcal{I}_{comp} , as the independent variable. In view of the one-to-one relation between \mathcal{I}_{comp} and \mathcal{I}_s , different compensator settings correspond to different choices of \mathcal{I}_s . In particular, both the quad-Fryze compensator of [7] and the theoretically optimal compensator of [8] are described in terms of the desired \mathcal{I}_s (recall, e.g. (1)). This facilitates getting analytical results, but makes it rather difficult to implement these compensators.

Our main objective is to construct an adaptive compensation algorithm that is easy to implement (and hence specifies \mathcal{I}_{comp} directly), relies only on the phasor arrays \mathcal{I} and \mathcal{V} corresponding to the load, and converges to a steady-state that is very near the theoretical optimum. This means we wish to achieve in steady-state prescribed values of P_{load} and P_{comp} (usually $P_{comp} = 0$), while reducing P_{line} to almost its theoretical minimum. Moreover, our adaptive algorithm should be able to track changes in the line (and the load) characteristics.

III. OPTIMAL PERFORMANCE CURVES

In order to evaluate the performance of our adaptive compensation scheme in the presence of non-negligible source impedance, we shall use the concept of optimal performance curves, originally introduced in [8]. The first step towards the construction of such curves is to obtain explicit expressions for the three criteria of interest — P_{line} , P_{load} and P_{comp} — as a function of the source current \mathcal{I}_s .

Following the practice in [8] we use here the normalized independent vector variable

$$\mathcal{X} \stackrel{\text{def}}{=} \frac{1}{\sqrt{P_{nom}}} \mathcal{I}_s \mathcal{R}_s^{1/2} \quad (9a)$$

where P_{nom} is the nominal power that would be delivered to the load in the absence of the line impedance. This allows us to obtain the expressions

$$\frac{P_{line}}{P_{nom}} = \mathcal{X} \mathcal{X}^H = \|\mathcal{X}\|^2 \quad (9b)$$

and

$$\frac{P_{load}}{P_{nom}} = \mathcal{X} \xi^H + \xi \mathcal{X}^H - \mathcal{X} \mathcal{X}^H \quad (10a)$$

where

$$\xi \stackrel{\text{def}}{=} \frac{1}{2\sqrt{P_{nom}}} \mathcal{V}_s \mathcal{R}_s^{-H/2}. \quad (10b)$$

Notice that

$$\begin{aligned} \frac{P_{load}}{P_{nom}} &= 2\Re\{\mathcal{X} \xi^H\} - \frac{P_{line}}{P_{nom}} \\ &\leq 2\|\mathcal{X}\| \|\xi\| - \frac{P_{line}}{P_{nom}} \end{aligned} \quad (11)$$

which gives us the universal performance bound of [8], viz.,

$$\frac{P_{cloud}}{P_{nom}} \leq \sqrt{\frac{P_{sc}}{P_{nom}}} \cdot \sqrt{\frac{P_{line}}{P_{nom}}} - \frac{P_{line}}{P_{nom}} \quad (12)$$

where $P_{sc} \stackrel{\text{def}}{=} \mathcal{V}_s \mathcal{R}_s^{-1} \mathcal{V}_s^H$.

Thus feasible (P_{line}, P_{cloud}) combinations, under any compensation scheme, must satisfy the inequality (12), and correspond to points above the universal performance curve in Fig. 2. Notice that this curve depends only on the source voltage and impedance, and is completely independent of the load.

In contrast, the expression for P_{comp} is explicitly dependent on the load, as is the value of P_{nom} . The case of a linear load was analyzed in [8], where it was shown that

$$P_{nom} \stackrel{\text{def}}{=} \mathcal{V}_s \mathcal{G} \mathcal{V}_s^H \quad (13a)$$

where

$$\mathcal{G} \stackrel{\text{def}}{=} \frac{1}{2}(\mathcal{Y} + \mathcal{Y}^H), \quad (13b)$$

as well as

$$\frac{P_{comp}}{P_{nom}} = \mathcal{X} A \mathcal{X}^H - \mathcal{X} \eta^H - \eta \mathcal{X}^H + 1 \quad (14a)$$

where

$$A \stackrel{\text{def}}{=} I + (\mathcal{R}_s^{-1/2} \mathcal{Z}_s) \mathcal{G} (\mathcal{R}_s^{-1/2} \mathcal{Z}_s)^H \quad (14b)$$

and

$$\eta \stackrel{\text{def}}{=} \frac{1}{\sqrt{P_{nom}}} \mathcal{V}_s \left[\frac{1}{2} I + \mathcal{G} \mathcal{Z}_s^H \right] \mathcal{R}_s^{-H/2}. \quad (14c)$$

For a nonlinear load we can determine P_{comp} only by numerical calculation, which solves the nonlinear equations that determine the map $\mathcal{I}_s \rightarrow \mathcal{V} \rightarrow \mathcal{I} \rightarrow \mathcal{I}_{comp} \rightarrow P_{comp}$ (See Appendix A).

Our main objective here is to determine *cross-section curves* corresponding to fixed values of P_{comp} . A cross-section curve defines the smallest possible value of P_{line} , as a function of P_{cloud} , for all compensators that achieve a prescribed value of P_{comp} . Here we shall limit our discussion to linear loads, for which one needs to solve a quadratic cost, quadratically-constrained optimization problem. As explained in [8], this can be accomplished via the Lagrange multiplier method, resulting in the optimal (scaled) source current

$$\mathcal{X}_{opt} = (\nu \xi + \lambda \eta) [(1 + \nu)I + \lambda A]^{-1} \quad (15)$$

where ν, λ are the Lagrange multipliers. Cross-section curves are obtained by finding all the (ν, λ) pairs that satisfy the constraint

$$\mathcal{X}_{opt} A \mathcal{X}_{opt}^H - 2\Re\{\mathcal{X}_{opt} \eta^H\} + 1 = \frac{P_{comp}}{P_{nom}} \quad (16)$$

for a given P_{comp} value.

One way to accomplish that is by searching the (ν, λ) plane along radial directions. In other words, we use a polar representation of the Lagrange multipliers, viz.,

$$\nu = \rho \sin \phi \quad , \quad \lambda = \rho \cos \phi \quad (17)$$

and search for the prescribed value of P_{comp} by varying ρ for a fixed value of ϕ . This results in a set of $(\nu(\phi), \lambda(\phi))$

pairs representing a given constant value for P_{comp} , say $P_{comp} = 0$. When P_{line} and P_{cloud} are evaluated using these $(\nu(\phi), \lambda(\phi))$ pairs of values we get the desired cross-section curve, representing $P_{line, opt}$ as a function of P_{cloud} for a fixed P_{comp} (see Fig. 2). This can be repeated for several useful values of P_{comp} . The cross-section curves described in Fig. 2 allow us to obtain the best trade-off between P_{line} and P_{cloud} achievable for the compensator whether it is supplying power, consuming power, or working under lossless conditions.

As an example, consider the case of a three-phase induction machine rated at $25kW$, supplied from an unbalanced source (variations of roughly 10% in magnitude and phase, with no zero sequence) that contains the fundamental and the fifth harmonic. The numerical values, which are the same as in [7], are provided in Appendix B.

We now observe that the smallest P_{line} achievable with a lossless compensator (dotted line in Fig. 2) is $1,418W$ and the corresponding $P_{cloud} = 18,660W$. If we attempt to supply the nominal power to the load, which in our example corresponds to $P_{cloud} = 22,750W$, then it is necessary to compromise on the power loss in the source impedance, i.e., P_{line} has to be increased to $2,376W$.

The family of all possible cross-section curves, for all possible values of P_{comp} is bounded from below by the universal performance bound given by (12). This boundary curve (solid line in Fig. 2) corresponds to the smallest P_{line} that can be achieved for a prescribed P_{cloud} , with no constraints imposed to the value of P_{comp} . It can also be determined directly from (15) by setting $\lambda = 0$.

IV. QUAD-FRYZE COMPENSATION

Our proposed adaptive compensation scheme is based on the concept of quad-Fryze compensation [7]. A quad-Fryze compensator is one that achieves, in steady-state,

$$i_s(t) = \alpha v(t) - \beta \mathcal{H}\{v(t)\}, \quad (18a)$$

for some constants α, β . In the frequency domain this translates into

$$\mathcal{I}_s = \gamma \mathcal{V}, \quad \gamma = \alpha + j\beta. \quad (18b)$$

This means that the compensated polyphase load is linear, time-invariant and balanced with no coupling between phases, and with a constant star-connected admittance equal to γ . When $\beta = 0$ this is simply a star-connected balanced, resistive load which is indeed the ideal load in situations where $\|\mathcal{V}_s - \mathcal{V}\| \ll \|\mathcal{V}_s\|$. However, allowing for $\beta \neq 0$ makes it possible to “fine-tune” the quad-Fryze compensator in the presence of a non-negligible (but not excessively large) line impedance.

The steady-state phasor relation (18b) implies, in conjunction with (4b), that the voltage across the load is given by

$$\mathcal{V} = \mathcal{V}_s (I + \gamma \mathcal{Z}_s)^{-1} \quad (19)$$

for the most general (e.g., nonlinear) load. Notice that \mathcal{I}_s , and consequently \mathcal{V} , rely on two real-valued design parameters — α and β — which makes it possible to satisfy the two desired constraints on P_{comp} and P_{cloud} . Actually, there exists a one-to-one correspondence between the pair (α, β) and the pair

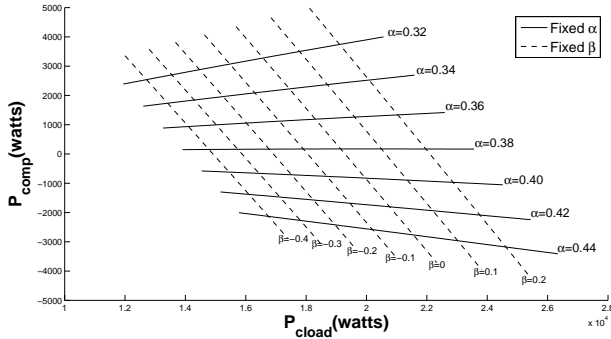


Fig. 3. Mapping of α, β into P_{comp} - P_{load} plane.

(P_{comp}, P_{load}), as illustrated in Fig. 3. Notice that lines of constant α are almost straight lines, all appearing to emanate from the origin ($P_{load} = 0 = P_{comp}$). In particular, the line $\alpha = 0.38$ very nearly corresponds to $P_{comp} = 0$: this suggests that our objective of lossless compensation can be achieved by controlling the value of α . Once the constraint of $P_{comp} = 0$ has been satisfied (in this example by setting $\alpha \approx 0.38$), we are free to vary the value of β so as to achieve a desired value of P_{load} . Notice that the relation between β and P_{load} , along a line of constant α , is monotone increasing. For instance, selecting β in the range $0 \leq \beta \leq 0.2$ (with $\alpha = 0.38$) results in P_{load} values in the range $19.1KW \leq P_{load} \leq 22KW$. Furthermore, we notice that it is possible to adjust β so that $P_{load} = P_{nom} = 22,750W$ while $P_{comp} = 0$.

The plotting of Fig. 3, and the choices for α and β values rely on specific information about network and load parameters, which makes a direct implementation of the quad-Fryze compensator rather impractical. However, our *adaptive algorithm* adjusts the values of α and β to achieve the prescribed P_{comp} and P_{load} values, relying in the process only on measurements of the load current and voltage (see Sec. V).

The values of P_{line} , P_{comp} and P_{load} associated with a quad-Fryze compensator can be evaluated via (19) and the expressions (6) – (8). Thus

$$P_{line} = |\gamma|^2 \mathcal{V} \mathcal{R}_s \mathcal{V}^H, \quad P_{load} = \alpha \|\mathcal{V}\|^2 \quad (20a)$$

for any load. Also, for a *linear load*,

$$P_{comp} = \mathcal{V}(\mathcal{G} - \alpha I)\mathcal{V}^H. \quad (20b)$$

In particular, in a *single-phase* system with sinusoidal excitation and a linear load we observe that $P_{comp} = (g - \alpha)|V|^2$, where “ g ” is the load conductance and “ V ” is the (scalar) phasor associated with the load voltage. In this very special case $P_{comp} = 0$ is achieved by setting $\alpha = g$, regardless of the value of β . Our polyphase, poly-harmonic example (Fig. 3) demonstrates that the same relation, namely $P_{comp} = 0 \iff$ constant α value, is still valid in general, so long as the voltage drop index $\frac{\|\mathcal{V}_s - \mathcal{V}\|}{\|\mathcal{V}_s\|}$ does not exceed several percent. In our example, this voltage drop index is around 16%.

The quad-Fryze compensator becomes optimal (with $\beta = 0$) when $\frac{\|\mathcal{V}_s - \mathcal{V}\|}{\|\mathcal{V}_s\|} \downarrow 0$. However, we will demonstrate via an

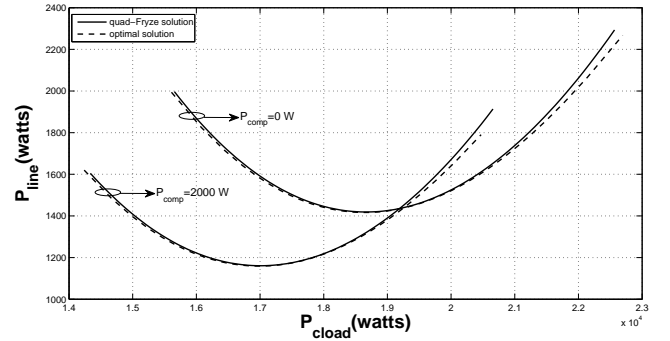


Fig. 4. Comparison between a quad-Fryze compensator solution versus an optimal solution ($P_{nom} = 22,750W$).

example in Sec. V that it is very nearly optimal even in the presence of a non-negligible line impedance. Indeed, the quality of the “match” between quad-Fryze and theoretically optimal performance depends on how “non-negligible” \mathcal{Z}_s is.

The expressions (20) allow us to determine the quad-Fryze equivalent of the cross-section curves of Fig. 2, i.e., the $P_{line} - P_{load}$ tradeoff achieved by a quad-Fryze compensator with a prescribed value of P_{comp} . The results for our induction machine example indicate that the performance of the quad-Fryze compensator is almost indistinguishable from the theoretical optimum (see Fig. 4, solid curves represent quad-Fryze solutions while dashed curves represent optimal solutions), i.e., less than 3% of difference between quad-Fryze and optimal P_{line} values when $0.60P_{nom} \leq P_{load} \leq P_{nom}$ for all P_{comp} . Notice that the best match between quad-Fryze and optimal curves is around the minimum point of the cross-section curves.

The basic challenge is to implement the quad-Fryze compensator, i.e., to find \mathcal{I}_{comp} such that $\mathcal{I}_s = \gamma\mathcal{V}$ is achieved without knowing \mathcal{Z}_s or the load characteristics. We can rely however on our ability to measure \mathcal{I} , \mathcal{V} whenever needed. In the following section we present an adaptive version of the quad-Fryze compensator that uses only \mathcal{I} , \mathcal{V} .

V. ADAPTIVE NEAR-OPTIMAL COMPENSATOR

The adaptive algorithm that we introduce in this section aims to enforce the quad-Fryze constraint $\mathcal{I}_s = \gamma\mathcal{V}$ in steady state. This is achieved by a repeated application of the compensation rule

$$\mathcal{I}_{comp}(k+1) = \mathcal{I}(k) - \gamma\mathcal{V}(k). \quad (21)$$

Each time we change the current supplied by the compensator, i.e., from $\mathcal{I}_{comp}(k)$ to $\mathcal{I}_{comp}(k+1)$, the load current and voltage experience a transient and eventually stabilize at a new set of values $\{\mathcal{I}(k+1), \mathcal{V}(k+1)\}$. Once the transient has died-off we can apply (21) again to set \mathcal{I}_{comp} to a new value.

Thus, the iteration (21) generates a sequence $\{\mathcal{I}, \mathcal{V}\}$ of load current-voltage pairs that converges (under mild technical constraints) to an equilibrium point of (21). This equilibrium is

$$\mathcal{I}_s(\infty) = \mathcal{I}(\infty) - \mathcal{I}_{comp}(\infty) = \gamma\mathcal{V}(\infty).$$

so that our objective of implementing quad-Fryze compensation, for a prescribed value of γ , is achieved.

The rate of convergence is determined by the voltage drop across the line impedance: higher values of the relative voltage drop $\|\mathcal{V}_s - \mathcal{V}\| / \|\mathcal{V}_s\|$ result in slower convergence. When this relative voltage drop is negligible our iteration (21) converges in a few steps (ideally in a single step).

We now turn to study the conditions for convergence of our iterative adjustment procedure (21).

A. Equilibrium and convergence

The dynamics of the compensator-load system can be described in terms of two maps:

- the iteration (21), which maps $\{\mathcal{I}(k), \mathcal{V}(k)\}$ into a new compensator current $\mathcal{I}_{comp}(k+1)$.
- the response of the network (including the load), which maps $\mathcal{I}_{comp}(k+1)$ into a new current-voltage pair $\{\mathcal{I}(k+1), \mathcal{V}(k+1)\}$.

This closed-loop feedback system is said to be in equilibrium if setting the compensator current according to (21) results in no transients and no change in the load current and voltage. Thus equilibrium is characterized by $\mathcal{I}_{comp} = \mathcal{I} - \gamma\mathcal{V}$ or, equivalently, $\mathcal{I}_s \equiv \mathcal{I} - \mathcal{I}_{comp} = \gamma\mathcal{V}$, which corresponds to quad-Fryze compensation. Notice that for a fixed γ this is unique, because we know from Sec. IV that the condition $\mathcal{I}_s = \gamma\mathcal{V}$ is satisfied by a single set of voltages and currents determined by $\mathcal{V} = \mathcal{V}_s(I + \gamma\mathcal{Z}_s)^{-1}$. Recall that the collection of the equilibrium points as a consequence of the implementation of the quad-Fryze policy for predetermined values of γ describes a curve that is nearly optimal as seen in Fig. 4.

We turn now our discussion to the convergence analysis of our adaptive compensator. When the load is linear we can use (5b) to establish a simple expression for the network response, viz.,

$$\mathcal{V}(k+1) = [\mathcal{V}_s + \mathcal{I}_{comp}(k+1)\mathcal{Z}_s][I + \mathcal{Y}\mathcal{Z}_s]^{-1}, \quad (22)$$

which, combined with (21) results in a linear difference equation for the load voltage, viz.,

$$\mathcal{V}(k+1) = \mathcal{V}(\infty) - \mathcal{V}(\infty)\mathcal{A} + \mathcal{V}(k)\mathcal{A}, \quad (23a)$$

where

$$\mathcal{V}(\infty) \stackrel{\text{def}}{=} \mathcal{V}_s(I + \gamma\mathcal{Z}_s)^{-1} \quad (23b)$$

and

$$\mathcal{A} \stackrel{\text{def}}{=} (\mathcal{Y} - \gamma I)\mathcal{Z}_s(I + \mathcal{Y}\mathcal{Z}_s)^{-1}. \quad (23c)$$

A detailed derivation is provided in Appendix C. This can be further simplified to

$$\epsilon(k+1) = \epsilon(k)\mathcal{A} \quad , \quad \epsilon(k) \stackrel{\text{def}}{=} \mathcal{V}(k) - \mathcal{V}(\infty), \quad (24)$$

which admits the explicit solution $\epsilon(k) = \epsilon(0)\mathcal{A}^k$. It is well known that $\|\epsilon(k)\| \rightarrow 0$ if, and only if, all the eigenvalues of \mathcal{A} are strictly within the unit circle, namely, $\max\{|\lambda_i(\mathcal{A})|\} < 1$. For the case when γ is fixed, our convergence analysis reduces to the examination of the eigenvalues of the constant matrix \mathcal{A} . In particular, we can explore this ‘‘convergence region’’ in terms of α, β as shown in Fig. 5 for our example. Notice that the range of α, β values shown in Fig. 3, namely

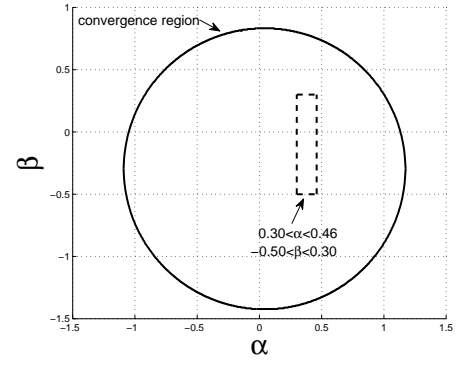


Fig. 5. Convergence region in terms of α, β for $\max\{|\lambda_i(\mathcal{A})|\} \leq 1$.

$0.30 \leq \alpha \leq 0.46$ and $-0.50 \leq \beta \leq 0.30$, is well within this convergence region.

Our next step is to propose an *adaptive adjustment* of α that will produce a prescribed value of P_{comp} (most often $P_{comp} = 0$) using only $\mathcal{I}(k), \mathcal{V}(k)$ and β values. Once the desired value of P_{comp} has been achieved we shall turn to obtain a desired value of P_{load} by adjusting β . During this process we rely only on relations that involve \mathcal{I}, \mathcal{V} (and γ), but nothing else.

B. Adaptive adjustment of α

The complex scalar γ in our iterative procedure (21) can be used to control the steady state values of both P_{comp} and P_{load} , as suggested by our preliminary analysis in Sec. IV (recall Fig. 3). We propose to use an adjustable value of α given by

$$\alpha(k) = \Re\{\gamma(k)\} = \frac{\Re\{\mathcal{I}(k)\mathcal{V}^H(k)\} - P_{comp,desired}}{\|\mathcal{V}(k)\|^2} \quad (25)$$

with the objective of enforcing a prescribed value on P_{comp} (which constitutes a priority over enforcing P_{load} in this step). This expression is motivated by the observation that in steady state

$$P_{load} = \alpha\|\mathcal{V}\|^2 = \Re\{\mathcal{I}\mathcal{V}^H\} - P_{comp},$$

which follows from (8) and (20a).

This means that our adaptive algorithm is, in fact,

$$\mathcal{I}_{comp}(k+1) = \mathcal{I}(k) - [\alpha(k) + j\beta]\mathcal{V}(k), \quad (26)$$

with $\alpha(k)$ given by (25). This recursion has the same unique equilibrium point as (21), namely $\mathcal{I}_s(\infty) = \gamma(\infty)\mathcal{V}$, so that (recall (8) and (20a))

$$\begin{aligned} P_{comp}(\infty) &= \Re\{\mathcal{I}(\infty)\mathcal{V}^H(\infty)\} - \alpha(\infty)\|\mathcal{V}(\infty)\|^2 \\ &= P_{comp,desired} \end{aligned}$$

where we also used (25) with $k = \infty$.

C. Adjustment of β

We now turn to select a value for the parameter β in (26) so as to achieve the desired level of P_{load} in equilibrium. When the line and load parameters $\mathcal{Z}_s, \mathcal{Y}$ are known, we

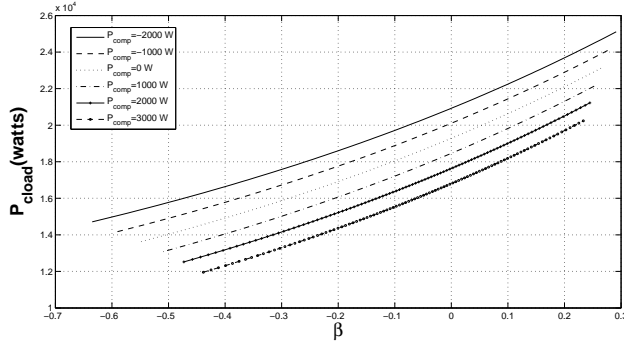


Fig. 6. P_{cloud} versus β for different values of P_{comp} .

can determine the explicit relation between P_{cloud} and β (Fig. 6). Because this relation is smooth and monotone increasing, one can use a variety of search procedures to determine the correct β for a desired P_{cloud} value. However, our objective is to develop a procedure for adjusting β that does not rely on knowledge of either \mathcal{Z}_s or \mathcal{Y} .

From a mathematical standpoint, our problem is to solve the (nonlinear) equation $f(\beta) = P_{cloud,desired}$, where $f(\cdot)$ is the monotone increasing function shown in Fig. 6. This could be done, for instance, via a Newton-Raphson type procedure when an explicit expression for $f(\beta)$ is available. However, since our goal is to rely on measurable quantities — namely \mathcal{I} , \mathcal{I}_s and \mathcal{V} — we need to use an “equation free” approach, such as the *secant method*, viz.,

$$\beta_{i+1} = \beta_i - \frac{\beta_i - \beta_{i-1}}{\bar{P}_{cloud,i} - \bar{P}_{cloud,i-1}} [\bar{P}_{cloud,i} - \bar{P}_{cloud,desired}], \quad (27a)$$

For computational convenience we use here normalized P_{cloud} values, viz.,

$$\bar{P}_{cloud} = \frac{P_{cloud}}{P_{nom}}. \quad (27b)$$

so that $\bar{P}_{cloud,i}$ is the normalized value of P_{cloud} achieved with β_i .

A graphical illustration of the secant method is provided in Fig. 7 starting with two given input-output pairs (points [1] and [3]) to determine a straight line connecting these points. This approximates the tangent line used in a Newton-Raphson type procedure. Next, we extend this line until it intersects (at point [4] in Fig. 7) the level $P_{cloud,desired}$ and determines the corresponding β_2 value.

Notice that the recursion (27a) is initialized with a choice of β_0 and β_1 . A reasonable choice for β_0 would be $\beta_0 = 0$, since it tends to generate a near-optimal value for the line loss P_{line} (see Fig. 8a). The selection of β_1 has to be consistent with the monotone increasing nature of the curves in Fig. 6, so that $\beta_1 > \beta_0$ when $P_{cloud,desired} > P_{cloud,0}$, which is usually the case. One possible choice for β_1 is via the expression $\frac{\beta_1}{\alpha_0(\infty)} = \tan(\Phi)$, where Φ is some problem-independent choice. For instance, the value in Table I was obtained with $\Phi = 35^\circ$. More research is needed to determine a universally efficient choice for Φ .

In summary, our adaptive compensation algorithm operates in two time scales:

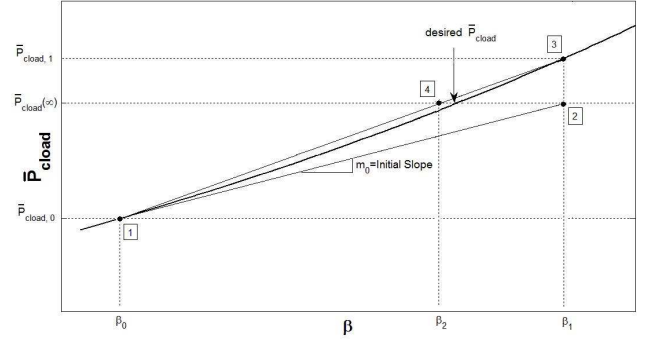


Fig. 7. Iterative adjustment of β to get desired \bar{P}_{cloud} .

- fast time scale (steps): for each β_i we run the adaptive algorithm (26) producing a sequence of $\alpha_i(k)$ values until convergence is achieved with $\alpha_i(k) \rightarrow \alpha_i(\infty)$. The value of β remains fixed (at β_i) throughout this transient adjustment process.

- slow time scale (stages): we determine β_{i+1} via (27a), using β_i , β_{i-1} and the steady state value $P_{cloud,i}(\infty) = \alpha_i(\infty) \|\mathcal{V}_i(\infty)\|^2$ achieved when (26) has converged.

Once the value of β is changed from β_i to β_{i+1} the system is no longer in equilibrium: the value of α has to be readjusted using (26), (25) until a new equilibrium is achieved, with a new value of P_{cloud} , as well as new load current and voltage, and a new value of P_{line} .

Table I shows the sequence of steady-state α , P_{line} , P_{cloud} , P_{comp} values associated with the β_i for $i = 0, 1, 2, 3$. Notice that the steady state $\alpha_i(\infty)$ values are practically independent of the β_i values: this is consistent with our observations in Section IV about Fig. 3. Also notice that the desired P_{cloud} is achieved after three adjustments of β , while $P_{comp} = 0$ is maintained.

TABLE I
STEADY-STATE VALUES AT THE END OF EACH SEGMENT OF THE TRAJECTORY (DOTTED LINE) IN FIG. 8A

Eq. point	β	α	P_{line}	P_{cloud}	P_{comp}
uncomp.	—	—	1,944W	16,080W	0
0	0	0.383443	1,442W	19,286W	0
1	0.269715	0.382797	2,591W	23,199W	0
2	0.238770	0.382872	2,354W	22,704W	0
3	0.241666	0.382859	2,375W	22,750W	0

The gradual adjustment process achieved by our adaptive algorithm is illustrated in Fig. 8, which shows both steady state points (shown by ‘o’ marks) and transient points (shown by ‘x’ marks). A dotted line connects the various points, defining a trajectory in the P_{cloud}/P_{line} plane. Notice that the steady-state points lie exactly on the quad-Fryze cross section curve corresponding to $P_{comp} = 0$ (solid line in Fig. 8b), while the transient points do not. Thus P_{line} achieves its near-optimal value in the i -th segment only when $\alpha_i(k)$ has converged. During the transient stage of $\alpha_i(k)$ adjustment, P_{line} can be quite different from its optimal value.

The convergence trajectory starts under conditions of an

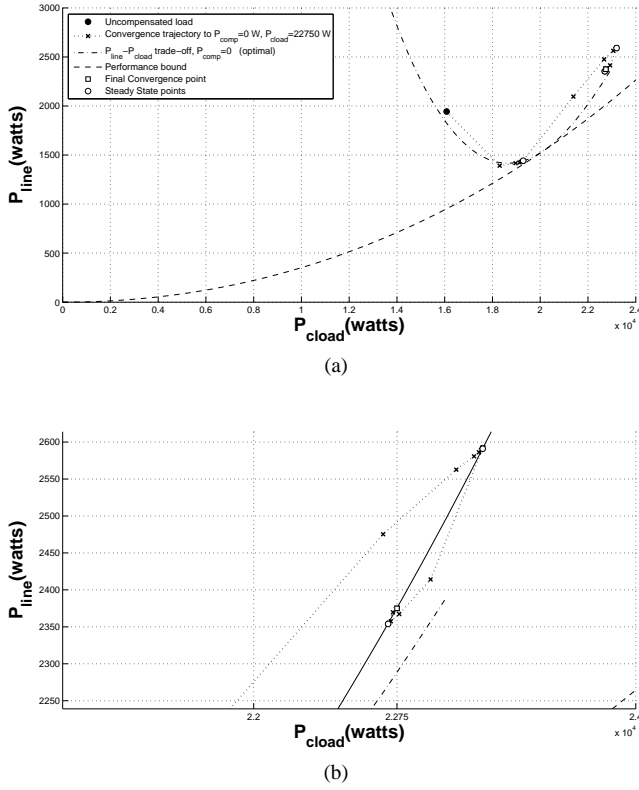


Fig. 8. (a) Convergence trajectory of the adaptive near-optimal compensator for $P_{\text{comp}}(\infty) = 0$, $P_{\text{load}}(\infty) = 22,750W$. (b) Zoomed-in view of the final adaptation stage. Solid line represents quad-Fryze solution for the $P_{\text{line}} - P_{\text{load}}$ trade-off when $P_{\text{comp}}(\infty) = 0$.

uncompensated load (black circle in Fig. 8a): in the absence of the compensator, the power loss in the source impedance of our example is $1,944W$, and the power delivered to the load is $16,080W$. The first steady state point, achieved with $\beta_0 = 0$, lies very near the minimum of the cross section curve. Notice that β (and P_{load}) keep increasing during the initial β -search steps, but eventually oscillate up and down until convergence is achieved with $P_{\text{load}}(\infty) = P_{\text{load,desired}} = 22,750W$, where it is clear that our ability to enforce a desired value for P_{load} (in this example $P_{\text{load,desired}} = P_{\text{nom}}$) comes at the expense of an increase in P_{line} .

D. Transient behavior

During the transient stage of $\alpha(k)$ convergence all three power quantities — P_{line} , P_{comp} , P_{load} — undergo a transient while $\alpha(k)$ is being adjusted. The transient behavior of P_{line} and P_{load} is evident in Figs. 8a, 8b (shown by ‘x’ marks). However, in order to observe the transient in P_{comp} we will use a separate P_{comp} vs. P_{load} plot (Fig. 9).

Notice that P_{comp} experiences a significant overshoot (dashed line in Fig. 9) at the beginning of each adaptation stage, right after the value of β is changed (namely from $k = 0$ to $k = 1$ in (26)). This overshoot is particularly noticeable in the first two adaptation stages (β_0 and β_1). This overshoot violates our objective of maintaining $P_{\text{comp}}(k) \approx P_{\text{comp,desired}}$ throughout the adaptation process. In particular, notice that in our example, with $P_{\text{comp,desired}} = 0$, there is one instant

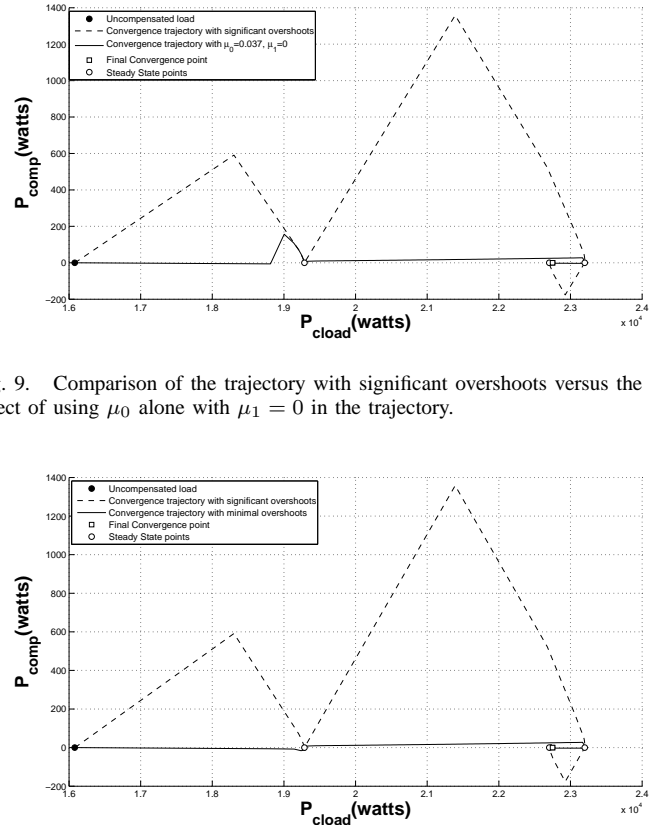


Fig. 9. Comparison of the trajectory with significant overshoots versus the effect of using μ_0 alone with $\mu_1 = 0$ in the trajectory.

Fig. 10. Comparison of the trajectory with significant overshoots versus the trajectory with minimal overshoots.

in which the compensator is required to supply more than $1,300W$.

This problem can be mitigated by a short-term increase in the value of $\alpha(k)$, since higher α -values result in lower P_{comp} values (recall Fig. 3). This can be achieved, for instance, by including additional temporary scaling of the value of $\alpha(k)$, but maintaining the recursion formula (26) as before, so that

$$\gamma(k) = [1 + \mu(k)]\alpha(k) + j\beta, \quad (28)$$

where $\mu(k) \rightarrow 0$ as $k \rightarrow \infty$.

When the values of \mathcal{Z}_s and \mathcal{Y} are known in advance, the sequence $\mu(k)$ can be chosen to optimize the performance, i.e., reduce the “overshoots” and “undershoots” in terms of the difference between $P_{\text{comp}}(k)$ and $P_{\text{comp,desired}}$.

From Fig. 3, it is intuitively plausible to think that to get $P_{\text{comp}} \downarrow$ we need to increase α , hence $\mu(k) > 0$, especially at the beginning of the iteration process. Since the overshoot occurs mostly in the first adaptation step (i.e., for $k = 0$ in (26)), one simple choice for $\mu(k)$ is to set $\mu(k) \neq 0$ only for $k = 0$. However, this still leaves a residual overshoot in the first segment of trajectory when $\beta = 0$, albeit a smaller one (solid line in Fig. 9), so that we opt to use

$$\mu(k) = \begin{cases} \mu_0, & k = 0 \\ \mu_1 \eta^{k-1}, & k \geq 1, \end{cases} \quad (29)$$

which leaves us with the challenge of selecting μ_0 , μ_1 and η without relying on prior information about network and/or

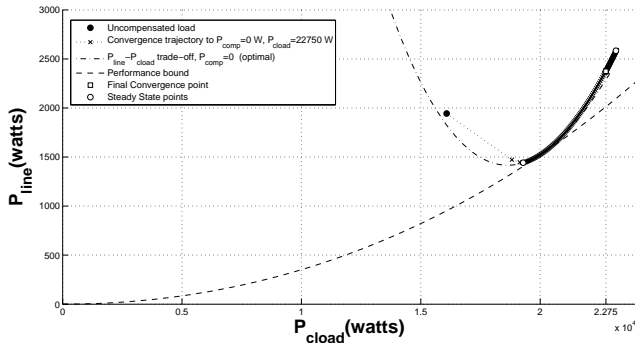


Fig. 11. Convergence trajectory with minimal overshoots of P_{comp} .

load parameters. Though optimal adaptive selection of μ_0 , μ_1 , η is still an open research problem, we are able to demonstrate that (29) can dramatically reduce the undesired overshoot in P_{comp} .

We found by trial and error that the values $\mu_0 = 0.037$, $\mu_1 = 0.0095$, and $\eta = 0.67$ appear to work well in our example, resulting in an almost unnoticeable P_{comp} transient (solid line in Fig. 10). Notice that in our example the first overshoot to be mitigated will be the same no matter what is the desired P_{cload} (taking into account that our interest is focused on situations where $P_{comp,desired} = 0$) since our adaptive algorithm is starting with $\beta = 0$.

We have found that the technique (28) and (29) works well during the first adaptation stage (with $\beta_0 = 0$). To overcome the overshoot in subsequent β -search stages we chose instead to implement the change from β_i to β_{i+1} , as given by (27a), not in a single step but as a sequence of smaller changes, each one of size $\frac{\beta_{i+1} - \beta_i}{M_{i+1}}$, where we chose $M_1 = 55$ and $M_i = 10$ for $i \geq 2$. Notice that increasing M_i reduces the overshoot in the (i)-th stage, but increases the number of α -adjustment steps for this stage. Our choices represent a tradeoff between these two competing measures of performance. The effect of these choices can be appreciated in Fig. 10 (solid line) where we can observe that the overshoots in all β -search steps have been significantly reduced.

Figure 11 presents the performance of the convergence trajectory in the P_{line}/P_{cload} plane where it is evident that the reduction of P_{comp} overshoots results in a smoother adaptation trajectory, as compared with the one in Fig. 8a. In addition, observe that after the first segment of the trajectory the adaptive algorithm is very nearly on the theoretical optimum (dash-dot line), even during adaptation transients.

VI. CONCLUDING REMARKS

Our adaptive procedure scheme for load compensation in an (unbalanced) polyphase power system relies only on instantaneous (dynamic) phasors obtained from measurements of the load voltage and current. It achieves nearly optimal performance even when the source impedance is not negligible in comparison with the load impedance. We used the notion of cross section curves, derived from the theoretically-optimal performance bounds of [7], [8], to demonstrate the near-optimality of our compensation scheme.

Our adaptive compensation scheme converges to a “quad-Fryze” steady state mode of operation, in which the compensated line current $i_s(t)$ is a linear combination of the load voltage $v(t)$ and its Hilbert transform $\mathcal{H}\{v(t)\}$. In the domain of phasors this relation is $\mathcal{I}_s = (\alpha + j\beta)\mathcal{V}$. We adjust the values of the control parameters α and β to achieve prescribed values for P_{comp} and P_{cload} , respectively. In particular, for $P_{comp} = 0$, our results show that the steady-state value of α is almost independent of the prescribed value of P_{cload} .

During the transient stage of our adaptation procedure the value of P_{comp} may deviate significantly from its desired steady-state value. We have outlined two distinct techniques for reducing such transient oscillations, and have demonstrated their ability to maintain manageable behavior during adaptation.

Optimality operation is hard to implement because it relies on \mathcal{Z}_s and \mathcal{Y} (and even harder for a nonlinear load), however it opens the possibility of networked collaboration as an implicit way of knowing \mathcal{Z}_s without measuring it and also improving compensation in general, which constitutes an ambitious challenge to be met in our following studies.

APPENDIX A RELATION BETWEEN \mathcal{I}_s AND \mathcal{I}_{comp}

In order to determine the polyphase load voltage $v(t)$ and load current $i(t)$ we need to consider the circuit equations

$$i(t) = i_s(t) + i_{comp}(t) \quad , \quad v_s(t) = v(t) + \mathcal{Z}_s \{i_s\}(t) \quad (30a)$$

and the load current-voltage relation

$$i(t) = \mathcal{Y}_\ell \{v\}(t) \quad . \quad (30b)$$

Here $\mathcal{Z}_s \{\cdot\}$ is an operator that describes the voltage-current relation of the source impedance, while $\mathcal{Y}_\ell \{\cdot\}$ denotes an operator that maps the voltage applied across the load into the resulting current flow through the load. While $\mathcal{Y}_\ell \{\cdot\}$ can, in general, be nonlinear, it is reasonable to assume that $\mathcal{Z}_s \{\cdot\}$ is a linear time-invariant operator. In the absence of a compensator, the load voltage and current satisfy the nonlinear equation

$$v_s(t) = v(t) + \mathcal{Z}_s \{\mathcal{Y}_\ell \{v\}\}(t) \quad , \quad (31)$$

which involves the *composition* of the operators $\mathcal{Y}_\ell \{\cdot\}$ and $\mathcal{Z}_s \{\cdot\}$. When a compensating current $i_{comp}(t)$ is present, the fundamental nonlinear equation, obtained by eliminating both $i_s(\cdot)$ and $i(\cdot)$ from (30a)-(30b) becomes

$$v_{se}(t) = v(t) + \mathcal{Z}_s \{\mathcal{Y}_\ell \{v\}\}(t) \quad , \quad (32)$$

where $v_{se}(t) \triangleq v_s(t) + \mathcal{Z}_s \{i_{comp}\}(t)$ acts as an equivalent source voltage, due to the presence of both $v_s(t)$ and $i_{comp}(t)$.

Equation (32) is a non-linear operator equation due to non-linearity of the load. In general, such equations have unique solutions subject to restrictions on the operators \mathcal{Z}_s , \mathcal{Y}_ℓ and the driving term $v_s(t) + \mathcal{Z}_s \{i_{comp}\}(t)$. For example, when the load is linear and $v_s(t)$, $i_{comp}(t)$ are periodic square integrable

waveforms, this equation can be written in terms of phasor arrays as

$$\mathcal{V}_s + \mathcal{I}_{comp} \mathcal{Z}_s = \mathcal{V} (I + \mathcal{Y} \mathcal{Z}_s) \quad , \quad (33)$$

so that a unique solution exists for any choice of \mathcal{V}_s and \mathcal{I}_{comp} as long as the matrix $(I + \mathcal{Y} \mathcal{Z}_s)$ is *invertible*.

From a practical perspective we know that the loads connected to the power grid always have a unique voltage developed across the load for given network conditions. In other words, the non-linear equation (32) always has a unique solution in the regime of normal power grid operation. Further research is needed to determine the precise mathematical conditions that need to be imposed on (32) to ensure the existence of a unique solution. For now, we shall adopt the working hypothesis that such conditions are indeed met in cases of practical interest.

One obvious case when uniqueness of solution is guaranteed is when the load is linear and $\|\mathcal{Y} \mathcal{Z}_s\| \ll 1$. In this case (33), the linear version of (32) under periodic conditions, has a unique solution because $(I + \mathcal{Y} \mathcal{Z}_s)$ is invertible. The condition $\|\mathcal{Y} \mathcal{Z}_s\| \ll 1$ expresses our assumption that the load impedance is much larger than the source impedance, resulting in a negligible voltage drop across the source impedance.

However, it is entirely possible to have a relatively small voltage drop even when the norm $\|\mathcal{Y} \mathcal{Z}_s\|$ is larger than one. For instance, according to the numerical values of the example in Appendix B we have $\|\mathcal{Y} \mathcal{Z}_s\| = 2.18$ while $\|\mathcal{V}_s - \mathcal{V}\| / \|\mathcal{V}_s\| \approx 0.16$ and $\min \{|\lambda_i(I + \mathcal{Y} \mathcal{Z}_s)|\} = 1.17$. It turns out that while the relative voltage drop $\|\mathcal{V}_s - \mathcal{V}\| / \|\mathcal{V}_s\|$ and the impedance-ratio $\|\mathcal{Y} \mathcal{Z}_s\|$ are very closely related in the sinusoidal single-phase case, this relation is much more flexible in the poly-harmonic, polyphase case.

Another interesting example of existence and uniqueness of a solution for the nonlinear circuit equations is analyzed in [15] in the context of a nonlinear resistive load. It is shown that in such a case, when the load is both upper and lower bounded by linear resistive loads, a unique solution for (32) exists subject to the following mild constraints:

- The source impedance is linear, time-invariant and BIBO stable.
- The polyphase waveform $v_s(t)$ (and $i_{comp}(t)$) is periodic and square integrable.

However, these conditions may not be sufficient when the nonlinear load is dynamic (i.e., non-resistive).

We now turn to analyze the effect of varying $i_{comp}(t)$ on the load conditions, assuming that $v_s(t)$ remains unchanged. When (32) has a unique solution $v(t)$, it defines a map $i_{comp}(t) \rightarrow v(t)$, which induces a map $i_{comp}(t) \rightarrow i_s(t)$, where we used the relations $i(t) = \mathcal{Y}_\ell \{v\}(t)$ and $i_s(t) = i(t) - i_{comp}(t) = \mathcal{Y}_\ell \{v\}(t) - i_{comp}(t)$. In fact, this map can be described by the implicit non-linear relation

$$i_{comp}(t) + i_s(t) = \mathcal{Y}_\ell \{v_s - \mathcal{Z}_s \{i_s\}\}(t) \quad , \quad (34)$$

which determines $i_s(t)$ uniquely in terms of $\{v_s(t), i_{comp}(t)\}$ whenever (32) admits a unique solution.

Moreover, whenever (34) admits a unique solution $i_s(t)$ it also establishes a one-to-one correspondence between $i_s(t)$

and $i_{comp}(t)$, for a predetermined $v_s(t)$. Indeed, for a given $i_s(t)$ in the range of solutions of (34) there can be only one $i_{comp}(t)$, given via (34) by

$$i_{comp}(t) = \mathcal{Y}_\ell \{v_s - \mathcal{Z}_s \{i_s\}\}(t) - i_s(t) \quad . \quad (35)$$

The one-to-one relationship $\mathcal{I}_{comp} \longleftrightarrow \mathcal{I}_s$ allows us to use \mathcal{I}_s as the independent optimization variable in Sec. III. However, it follows from the preceding discussion that choices of \mathcal{I}_s must be constrained to the range of solutions of (34).

In the linear case we know that (33) has a unique solution if, and only if, the matrix $(I + \mathcal{Y} \mathcal{Z}_s)$ is nonsingular. In this case (34) reduces to

$$\mathcal{I}_{comp} = -\mathcal{I}_s [I + \mathcal{Z}_s \mathcal{Y}] + \mathcal{V}_s \mathcal{Y} \quad , \quad (36)$$

which has a unique solution for \mathcal{I}_s under the same conditions, since

$$\det(I + \mathcal{Z}_s \mathcal{Y}) = \det(I + \mathcal{Y} \mathcal{Z}_s) \quad . \quad (37)$$

We conclude that in the linear case the correspondence $\mathcal{I}_{comp} \longleftrightarrow \mathcal{I}_s$ is well defined for all square summable \mathcal{I}_{comp} and \mathcal{I}_s , as long as $(I + \mathcal{Z}_s \mathcal{Y})$ is invertible.

APPENDIX B

NUMERICAL VALUES OF THE CASE OF STUDY

The numerical values of the load compensation example used in this paper are

$$\mathcal{V}_s = [\mathcal{V}_{s1} \quad \mathcal{V}_{s2} \quad \mathcal{V}_{s3} \quad \mathcal{V}_{s4} \quad \mathcal{V}_{s5} \quad \mathcal{V}_{s6}] \quad ,$$

where

$$\mathcal{V}_{s1} = 138.6, \quad \mathcal{V}_{s2} = -38.54 - 118.6j, \quad \mathcal{V}_{s3} = -100 + 118.6j, \\ \mathcal{V}_{s4} = 13.86, \quad \mathcal{V}_{s5} = -6.928 - 12j \text{ and } \mathcal{V}_{s6} = -6.928 + 12j.$$

$$\mathcal{Z}_s = 0.195 \begin{bmatrix} 1+2j & 0 & 0 & 0 & 0 & 0 \\ 0 & 1+2j & 0 & 0 & 0 & 0 \\ 0 & 0 & 1+2j & 0 & 0 & 0 \\ 0 & 0 & 0 & 1+10j & 0 & 0 \\ 0 & 0 & 0 & 0 & 1+10j & 0 \\ 0 & 0 & 0 & 0 & 0 & 1+10j \end{bmatrix} \quad ,$$

$$\mathcal{Y} = \begin{bmatrix} \mathcal{Y}_1 & 0 \\ 0 & \mathcal{Y}_5 \end{bmatrix} \quad ,$$

where

$$\mathcal{Y}_1 = \begin{bmatrix} 1.047 - 2.447j & 1.093 - 0.9531j & -0.2024 - 1.212j \\ -0.2024 - 1.212j & 1.047 - 2.447j & 1.093 - 0.9531j \\ 1.093 - 0.9531j & -0.2024 - 1.212j & 1.047 - 2.447j \end{bmatrix}$$

and

$$\mathcal{Y}_5 = \begin{bmatrix} 0.1464 - 0.8491j & -0.0212 - 0.1271j & -0.0347 - 0.1014j \\ -0.0347 - 0.1014j & 0.1464 - 0.8491j & -0.0212 - 0.1271j \\ -0.0212 - 0.1271j & -0.0347 - 0.1014j & 0.1464 - 0.8491j \end{bmatrix}$$

Notice that the phasors array \mathcal{V}_s and the matrices \mathcal{Y} and \mathcal{Z}_s consist of only the first and fifth harmonic components. The remaining components in this example are all zero.

The eigenvalues for the product $(\mathcal{Z}_s \mathcal{Y})$ are

$$\lambda_i(\mathcal{Z}_s\mathcal{Y}) = \begin{bmatrix} 2.1766 - 0.1437j \\ 0.1682 + 0.0999j \\ 1.1307 - 0.1627j \\ 2.1190 - 0.0337j \\ 1.4485 + 0.2424j \\ 1.4854 + 0.1510j \end{bmatrix}$$

so that $\Re\{\lambda_i\} > 0$ for all i .

APPENDIX C

DERIVATION OF DIFFERENCE EQUATION (23)

Using the linear load relation $\mathcal{I} = \mathcal{V}\mathcal{Y}$, we can deduce from (21) that the compensator current during the adaptation process is given by

$$\mathcal{I}_{comp}(k+1) = \mathcal{V}(k)[\mathcal{Y} - \gamma\mathcal{I}]. \quad (38)$$

Combining the compensator current setting (38) with the network response (22) results in a new load voltage

$$\mathcal{V}(k+1) = \mathcal{V}_s(I + \mathcal{Y}\mathcal{Z}_s)^{-1} + \mathcal{V}(k)\mathcal{A}, \quad (39a)$$

where

$$\mathcal{A} \stackrel{\text{def}}{=} (\mathcal{Y} - \gamma\mathcal{I})\mathcal{Z}_s(I + \mathcal{Y}\mathcal{Z}_s)^{-1}. \quad (39b)$$

The equilibrium point is given by (recall (19))

$$\mathcal{V}(\infty) = \mathcal{V}_s(I + \gamma\mathcal{Z}_s)^{-1} \quad (40)$$

which allows us to rewrite (39a) in the form of a linear difference equation for the load voltage, viz.,

$$\mathcal{V}(k+1) = \mathcal{V}(\infty) - \mathcal{V}(\infty)\mathcal{A} + \mathcal{V}(k)\mathcal{A}, \quad (41)$$

where we used the identity

$$\mathcal{V}(\infty)[I - \mathcal{A}] = \mathcal{V}_s(I + \mathcal{Y}\mathcal{Z}_s)^{-1}$$

which follows from (40) and the observation

$$\begin{aligned} I - \mathcal{A} &= [(I + \mathcal{Y}\mathcal{Z}_s) - (\mathcal{Y} - \gamma\mathcal{I})\mathcal{Z}_s][I + \mathcal{Y}\mathcal{Z}_s]^{-1} \\ &= (I + \gamma\mathcal{Z}_s)(I + \mathcal{Y}\mathcal{Z}_s)^{-1}. \end{aligned}$$

REFERENCES

- [1] A.A. Valdez, G. Escobar, R. Ortega, "An Adaptive Controller for the Shunt Active Filter Considering a Dynamic Load and the Line Impedance," *IEEE Trans. Control Syst. Technology*, Vol. 17, No. 2, pp. 458-464, March 2009.
- [2] D. Casadei, G. Grandi, C. Rossi, "Effects of Supply Voltage non-Idealities on the Behavior of an Active Power Conditioner for Cogeneration Systems," in *PESC 2000*, pp. 1312-1317.
- [3] S. Fryze, "Wirk-, Blind-, und Scheinleistung in electrischen Stromkreisen mit nichtsinusformigem Verlauf von Strom und Spannung," *Elektrotech. Z.*, Vol. 53, No. 25, pp. 596-599, June 1932.
- [4] H. Lev-Ari, A.M. Stanković, "Hilbert Space Techniques for Modeling and Compensation of Reactive Power in Energy Processing Systems," *IEEE Trans. Circuits Syst. I, Fundam. Theory Appl.*, Vol. 50, No. 4, pp. 540-556, Apr. 2003.
- [5] H. Lev-Ari, A.M. Stanković, K. Xu, M.M. Perišić, "Hilbert Space Techniques for Evaluating Trade-offs in Reactive Power Compensation," in *Proc. of the IEEE Int. Symp. on Circuits and Systems*, Vancouver, Canada, May 2004, Vol. V, pp. 976-979.
- [6] H. Lev-Ari, A.M. Stanković, "Hilbert Space Techniques for Reactive Power Compensation with Limited Current Bandwidth," *Proc. of the IEEE Int. Symp. on Circuits and Systems*, Vancouver, Canada, May 2004, Vol. V, pp. 904-907.

- [7] H. Lev-Ari, A.M. Stanković, "Optimizing Power Flows in Lossy Polyphase Systems: Effects of Source Impedance," *7th International Workshop on Power Definitions and Measurements under Non-Sinusoidal Conditions*, Cagliari, Italy, July 2006, pp. 78-83.
- [8] H. Lev-Ari, A.M. Stanković, "Fundamental Performance Limits in Lossy Polyphase Systems: Apparent Power and Optimal Compensation," *IEEE Int. Symp. on Circuits and Systems*, May 2007, Vol. 27, No. 30, pp. 61-64.
- [9] S.M.R. Rafiei and M.R. Iravani, "Optimal and adaptive compensation of voltage and current harmonics under nonstiff-voltage conditions," *IEE Proc.-Gener. Transm. Distrib.*, Sept. 2005, Vol. 152, No. 5, pp. 661-672.
- [10] S. R. Shaw, C. R. Laughman, S. B. Leeb and R. F. Lepard, "A Power Quality Prediction System", *IEEE Trans. Industrial Electronics*, Vol. 47, No. 3, pp. 511-517, June 2000.
- [11] J.F.G. Cobben and J.F.L. van Casteren, "Classification Methodologies for Power Quality", in *www.leonardo-energy.org*, Feb. 2006
- [12] M. Karimi-Ghatermani, S. A. Khajehoddin and A. Bakhshai, "Is the Unity Power Realizable at the Load Terminals?", *IEEE PES GM 2008*, Pittsburgh, PA
- [13] P. F. Ribeiro, "Common Misapplications of the IEEE 519 Harmonic Standard: Voltage or Current Limits", *IEEE PES GM 2008*, Pittsburgh, PA
- [14] W.H. Kersting, "Causes and Effects of Unbalanced Voltages Serving an Induction Motor", *Rural Electric Power Conference*, 2000, pp. B3/1-B3/8.
- [15] I.W. Sandberg, "On Truncation Techniques in the Approximate Analysis of Periodically Time-Varying Nonlinear Networks", *IEEE Trans. Circuit Theory*, Vol. 11, No. 2, pp. 195-201, June 1964.